ISSN 1674-1056
http://cpb.iphy.ac.cn
http://iopscience.iop.org/cpb
中国物理 B
Chinese Physics
中国物理 Chinese Physics B

An overview of thermoelectric films: Fabrication techniques, classification, and regulation methods

Jing-jing Feng(冯静静), Wei Zhu(祝薇), Yuan Deng(邓元)
Citation: Chin. Phys. B . 2018, 27(4): 047210. **doi:** 10.1088/1674-1056/27/4/047210

Journal homepage: http://cpb.iphy.ac.cn; http://iopscience.iop.org/cpb

What follows is a list of articles you may be interested in

Coherent charge transport in ferromagnet/semiconductor nanowire/ferromagnet double barrier junctions with the interplay of Rashba spin–orbit coupling, induced superconducting pair potential, and external magnetic field

Li-Jie Huang(黄立捷), Lian Liu(刘恋), Rui-Qiang Wang(王瑞强), Liang-Bin Hu(胡梁宾)
Chin. Phys. B . 2017, 26(7): 077201. **doi:** 10.1088/1674-1056/26/7/077201

Spin-filter effect and spin-polarized optoelectronic properties in annulene-based molecular spintronic devices

Zhiyuan Ma(马志远), Ying Li(李莹), Xian-Jiang Song(宋贤江), Zhi Yang(杨致), Li-Chun Xu(徐利春), Ruiping Liu(刘瑞萍), Xuguang Liu(刘旭光), Dianyin Hu(胡殿印)
Chin. Phys. B . 2017, 26(6): 067201. **doi:** 10.1088/1674-1056/26/6/067201

Current induced nonequilibrium spin polarization in semiconductor-nanowire/s-wave superconductor junctions with strong spin-orbit coupling

Nai-Qing Liu(刘乃清), Li-Jie Huang(黄立捷), Rui-Qiang Wang(王瑞强), Liang-Bin Hu(胡梁宾)
Chin. Phys. B . 2016, 25(2): 027201. **doi:** 10.1088/1674-1056/25/2/027201

Electronic band gap and transport in graphene superlattice with a Gaussian profile potential voltage

Zhang Yu-Ping, Yin Yi-Heng, Lü Huan-Huan, Zhang Hui-Yun
Chin. Phys. B . 2014, 23(2): 027202. **doi:** 10.1088/1674-1056/23/2/027202

The effect of *k*-cubic Dresselhaus spin–orbit coupling on the decay time of persistent spin helix states in semiconductor two-dimensional electron gases

Chai Zheng, Hu Mao-Jin, Wang Rui-Qiang, Hu Liang-Bin
Chin. Phys. B . 2014, 23(2): 027201. **doi:** 10.1088/1674-1056/23/2/027201

TOPICAL REVIEW — Recent advances in thermoelectric materials and devices

An overview of thermoelectric films: Fabrication techniques, classification, and regulation methods*

Jing-jing Feng(冯静静)[1], Wei Zhu(祝薇)[1,†], and Yuan Deng(邓元)[1,2,‡]

[1] School of Materials Science and Engineering, Beihang University, Beijing 100191, China
[2] Beijing Advanced Innovation Center for Biomedical Engineering, Beihang University, Beijing 100083, China

(Received 18 January 2018; revised manuscript received 9 March 2018; published online 29 March 2018)

Thermoelectric materials have aroused widespread concern due to their unique ability to directly convert heat to electricity without any moving parts or noxious emissions. Taking advantages of two-dimensional structures of thermoelectric films, the potential applications of thermoelectric materials are diversified, particularly in microdevices. Well-controlled nanostructures in thermoelectric films are effective to optimize the electrical and thermal transport, which can significantly improve the performance of thermoelectric materials. In this paper, various physical and chemical approaches to fabricate thermoelectric films, including inorganic, organic, and inorganic–organic composites, are summarized, where more attentions are paid on the inorganic thermoelectric films for their excellent thermoelectric responses. Additionally, strategies for enhancing the performance of thermoelectric films are also discussed.

Keywords: thermoelectric films, fabrication techniques, classification, regulation methods

PACS: 72.10.–d, 73.50.Lw, 81.15.–z, 84.60.Rb **DOI:** 10.1088/1674-1056/27/4/047210

1. Introduction

Seeking affordable, renewable energy and reducing dependence on carbon-based fossil energy have become main themes around the world.[1–3] Thermoelectric (TE) energy conversion has attracted widespread attention in recent years, which has widely potential applications such as mini-cooling systems, TE generators, and self-powered sensors.[4–8] Thermoelectricity can be traced back to 1821, when the German scientist Thomas Johann Seebeck observed the Seebeck effect, which is a fundamental effect for TE power generation. Later, the French physicist Jean Charles Athanase Peltier discovered the Peltier effect for TE cooling power refrigeration. The dimensionless figure of merit, zT ($zT = S^2\sigma T/k$, where S, σ, $S^2\sigma$, T, and k are Seebeck coefficient, electrical conductivity, power factor, absolute temperature, and total thermal conductivity, respectively), is an indicator to assess the performance of TE material, and many researchers devoted to the study of higher zT for expanding the role of TE materials in more practical applications.[9] However, only modest progress had been made for a long time until the early 1990s, when low-dimensional TE materials were predicted to have a much higher zT than bulk materials due to size effects and quantum confinement[10–14] Particularly, with the development of miniaturization, high integration and large power density in thermoelectric devices, the research of TE thin films has become a hot spot.

The thin-film TE material was originally developed among low-dimensional TE materials, including monolayer film and superlattice, which makes it easier to efficiently tailor electrical transport and thermal transport of TE materials. On one hand, the thin-film TE material can change the electronic density of state (DOS) by introducing the quantum effect.[10,15,16] On the other hand, the thermal conductivity can be largely reduced by phonon scattering at interface (film boundary and grain boundary) or phonon spectrum modification.[17,18] Koga *et al.*[19] reported that the superlattice period, layer thicknesses, and the superlattice growth direction can be used to optimize the zT of GaAs superlattice, which is much superior to bulk GaAs. A phonon-blocking/electron-transmitting structure in multiple-quantum-well Bi_2Te_3/Sb_2Te_3 superlattices has been fabricated and a highest zT value was obtained up to 2.4.[20] Consequently, higher performance can be achieved in well-controlled TE films, in virtue of its unique structural characteristics. TE films, including inorganic materials, organic materials, and inorganic–organic composites have been widely studied and many marvelous TE films have been commercialized.[21,22] In consideration of their relatively excellent TE properties, inorganic semiconductors materials have been extensively researched, which can be divided into three ranges according to the optimal working tem-

*Project supported by the Joint Funds of the National Natural Science Foundation of China (Grant No. U1601213), the National Natural Science Foundation of China (Grant Nos. 51601005 and 61704006), the Beijing Natural Science Foundation (Grant No. 2182032), and the Fundamental Research Funds for the Central Universities.

†Corresponding author. E-mail: zhu_wei@buaa.edu.cn
‡Corresponding author. E-mail: dengyuan@buaa.edu.cn

© 2018 Chinese Physical Society and IOP Publishing Ltd

perature region, namely low-temperature range (< 400 K) represented by Bi_2Te_3, medium-temperature range (600 K–900 K) represented by PbTe and high-temperature range (> 900 K) represented by Si–Ge.[23] Additionally, organic TE materials as well as inorganic–organic TE composites can also diversify the potential applications of thin-film TE devices.[24–26] To improve TE properties and design better TE films, many methods have been developed, such as vacuum evaporation,[27] sputtering,[28,29] pulsed laser deposition,[30] screen printing,[31] molecular beam epitaxy,[32] atomic layer deposition,[33] electrodeposition,[34,35] and so on. More importantly, tuning the carrier concentration, engineering the band structure, and suppressing the lattice thermal conductivity have also been considered to optimize the electrical and thermal transport of the films in essence.[12,17,36,37]

This paper is scheduled in the following way. First, various fabrication techniques of TE films, both chemical and physical methods will be introduced in the Section 2. Then, the different kinds of TE films, including inorganic (Section 3), organic and inorganic–organic composites (Section 4) will be summarized, especially the inorganic TE films which were described according to the optimal working temperature region in detail. Additionally, the strategies to optimize the property of TE films will be briefly reviewed in Section 5, paying particular attention to the oriented nanostructures to improve TE performance.

2. Fabrication of thermoelectric films

The processing techniques of TE films are classified into chemical and physical methods. For chemical methods, such as chemical vapor deposition and electrochemical deposition, precisely controlled TE films can be prepared, although these methods probably have environment hazards. For physical methods, like sputtering, molecular beam epitaxy, and screen printing, the microstructure and properties of TE films are relatively complicated to accurately control, because they entirely depend on the processing temperature, pressure, post-treatment, and so on.

2.1. Vacuum evaporation technique

Vacuum evaporation technique is a common physical vapor deposition used in the preparation of TE films, where evaporation source, substrate, and intermediate vacuum process play important roles in the performance optimization of the film. It includes co-evaporation and flash evaporation. Tan *et al.*[27] prepared a ternary compound n-type $Bi_2(Te,Se)_3$ nanowire array film on SiO_2 substrates through thermal co-evaporation technique, and zT value of 1.01 was achieved at room temperature. Highly oriented nanocrystalline $Bi_{0.4}Sb_{1.6}Te_3$ thin films were also fabricated by the flash evaporation.[38] In addition, Xu *et al.*[39] prepared SnTe thin films on the polished aluminum nitride substrates via one-step thermal evaporation method, and the maximum power factor of 19.8 $\mu W \cdot cm^{-1} \cdot K^{-2}$ was achieved owning to its special nanopillar structure. The process of evaporating TE films is simple, low-cost, and compatible with microelectronics process. However, the elemental composition is difficult to precisely control, especially when preparing thin-film materials with complex components, and meanwhile the fabricated films suffered from the weak adhesion with substrate.

2.2. Sputtering

In the sputtering process particles (solid atoms or molecules) are commonly ejected from a solid target material caused by the charged particles bombaring the solid surface (target). The sputtering process can be divided into four categories: direct current (DC), alternating current (AC), reactive and magnetron sputtering processes. Magnetron sputtering is extensively used in the preparation of TE films. Nanostructured $Si_{0.8}Ge_{0.2}$ films with different porous sizes were grown through DC sputtering processes and high TE power factor of 4.5 $\mu W \cdot cm^{-1} \cdot K^{-2}$ has been obtained.[40] Using DC magnetron sputtering, Sb_2Te_3 thin film with (015) crystal preferential orientation was obtained via directly depositing antimony telluride (Sb_2Te_3) on flexible polyimide substrate, which has a maximum power factor of 6.0 $\mu W \cdot cm^{-1} \cdot K^{-2}$.[28] And Na_xCoO_2 thin film was fabricated by an RF-magnetron sputtering method and achieved a power factor of 143 $\mu W \cdot cm^{-1} \cdot K^{-2}$.[41] Similarly, a series 500-nm-thick Sb_2Te_3 films were deposited onto SiO_2/Si substrates by radio frequency (RF) magnetron sputtering and the zT value reached approximately 1.5.[42] $CoSb_3$ skutterudite thin films with different Sb contents have been prepared by RF co-sputtering method, and a maximum power factor of 12.6 $\mu W \cdot cm^{-1} \cdot K^{-2}$ was obtained.[43] Meanwhile, through a simple magnetron co-sputtering method, Zhang *et al.*[44] fabricated highly (00l)-oriented Bi_2Te_3 thin films with in-plane layered columnar nanostructure. The films deposited by magnetron sputtering are dense, uniform, and typically own strong binding force with substrate. What is more, the TE films can be deposited at relatively low temperature and the microstructure can be well controlled by adjusting the kinetic energy of ionized ions.

2.3. Pulsed laser deposition (PLD)

Pulsed laser deposition, a versatile PVD technique, has been used to manufacture TE thin-film with high growth rates, multiple elements, and diverse structures and morphologies. The high-power pulsed laser beam generated by the excimer pulsed laser is focused on the target surface, leading to high temperature and erosion, and further high pressure plasma. The plasma is locally expanded and emitted. Subsequently, it is deposited on the substrate to form a thin film. Using a

Bi_2Se_2Te single crystal target, n-type nanocrystalline Bi–Se–Te thin films were deposited by PLD and owned an optimal power factor of 8.3 $\mu W \cdot cm^{-1} \cdot K^{-2}$.[30] And a series of iron doped bismuth selenide films were grown on Si (100) substrates using PLD at different substrate temperatures.[45] The PLD technique allows fine control of stoichiometry since it can grow a multi-compound film consistent with the target composition even the compound containing volatile elements. Due to the high concentration of laser energy, PLD can evaporate inorganic materials such as metal, semiconductor and ceramics, solving the problem of thin film deposition of refractory materials. However, it subjects certain restrictions in the large-scale preparation of TE films, owing to its difficulty to prepare large-area film.

2.4. Molecular beam epitaxy (MBE)

Molecular beam epitaxy can be utilized to prepare high-quality crystalline films on crystalline substrates in high vacuum or ultra-high vacuum (10^{-8} Torr$\sim 10^{-12}$ Torr, 1 Torr = 1.33322×10^2 Pa). Yoo *et al.*[46] prepared $Bi_2(Se_xTe_{1-x})_3$ films with different Se and Te concentrations on GaAs substrates through MBE method, and investigated the dependence of thermal conductivity on film composition. Meanwhile, they revealed that the $Bi_2(Se_xTe_{1-x})_3$ ternary alloys films had much lower thermal conductivity compared to those of $Bi_2Se_3$and Bi_2Te_3 films. What is more, a highly crystalline $Bi_{0.4}Sb_{1.6}Te_3$ film was deposited on Si substrate using MBE process,[47] and high-quality Sb_2Te_3 films were also prepared.[48] Using enhanced solid-source oxide MBE, Apreutesei *et al.* fabricated high-quality $La_{0.2}Sr_{0.8}TiO_3$ TE films on $SrTiO_3$ (001) substrates.[49] MBE can generally be carried out at low temperatures and precisely control the thickness, composition, structure, and doping concentration. Although MBE is remarkable to manufacture high-quality TE films, it has the limit of high cost and maintenance costs, overlong deposition time, and restriction in the large-scale application.

2.5. Printing fabrication techniques

Emerging studies on printing TE films have gained great attention owing to their simplicity and affordability. Compared with conventional manufacturing techniques, printing has relatively simple patterning, superior material compatibility, less time consuming, large-scale fabrication, and reduced energy input and material waste. So far, lots of printing techniques such as screen printing, inkjet printing, and direct writing have been focused on the fabrication of TE films and devices. For instance, through rationally optimizing the printing inks consisting of TE particles, binders, and organic solvents, Shin *et al.*[50] screen-printed TE films on flexible fiber glass fabrics, and relatively high room-temperature zT values of 0.65 (p-type $Bi_{0.5}Sb_{1.5}Te_3$) and 0.81 (n-type $Bi_2Te_{2.7}Se_{0.3}$) were achieved. TE films fabricated by inkjet printing of $Sb_{1.5}Bi_{0.5}Te_3$ and $Bi_2Te_{2.7}Se_{0.3}$ nanoparticles own the power factor of $\sim$0.77 $\mu W \cdot cm^{-1} \cdot K^{-2}$ (p-type) and 1.83 $\mu W \cdot cm^{-1} \cdot K^{-2}$ (n-type).[51] Using dispenser printer, Se doped Bi_2Te_3 (n-type) film and Te doped $Bi_{0.5}Sb_{1.5}Te_3$ (p-type) film were fabricated on a custom designed polyimide substrate, and further a TE generator was designed with a series-parallel prototype of 50 couples.[52]

2.6. Chemical vapor deposition (CVD)

Chemical vapor deposition is used to produce high-quality and high-performance solid materials, especially in the semiconductor industry. Generally, the substrate is exposed to volatile precursors, and then the volatile precursors will react and/or decompose on the substrate surface to produce the desired deposition. In CVD process, the produced volatile byproducts are usually removed by gas stream through the reaction chamber. CVD is implemented in a variety of formats, like metal–organic chemical vapor deposition (MOCVD), plasma enhanced chemical vapor deposition (PECVD), and low-pressure chemical vapor deposition (LPCVD), which are usually different in the initiation of the chemical reaction. A unique columnar grain structure p-type Si–Ge thin films synthesized by LPCVD was obtained with a high in-plane zT value of 0.2 at 300 K.[53] Through using MOCVD technique, Mahmood *et al.*[54] deposited ZnO thin films on a sapphire substrate and studied the influence of the annealing temperature on the property of ZnO films. In general, the TE film with high purity, little residual stress, and good crystallization can be obtained by using CVD method.

2.7. Atomic layer deposition (ALD)

Atomic layer deposition is a chemical fabrication technique of depositing thin-film on substrates by exposing their surfaces to alternate gaseous species (usually called precursors). Over time, ALD has been successfully applied to the thin films fabrication of semiconductors, metals, alloys, and oxides. Kim *et al.*[55] synthesized undoped ZnO thin films by ALD method, and concluded that using the strong oxidant-ozone, undoped ZnO film could get a higher power factor of 5.76 $\mu W \cdot cm^{-1} \cdot K^{-2}$ than 2.89 $\mu W \cdot cm^{-1} \cdot K^{-2}$ for the water-based ZnO film. In addition, Al_2O_3/ZnO superlattice thin films were deposited by ALD, and a relatively higher in-plane zT of 0.014 was achieved.[33] The TE films deposited by ALD have fewer impurities due to the surface reaction, regulatable thickness in angstrom scale by a self-limited reaction, and high quality by the self-limited reaction on the surface. However, ALD requires high consumption, long deposition time, and high requirements for precursors which should be volatile but not decomposed.

2.8. Electrodeposition

Electrodeposition, a process of coating by electrolysis, is analogous to a galvanic cell acting in reverse. So far, commonly used electrodeposition includes reaction deposition, co-deposition, and two-step deposition. Electrodeposition is attractive in the fabrication of TE films for its rapid, low-cost, and room-temperature process. Kim *et al.*[56] successively electrodeposited p-type Sb–Te and n-type Bi–Te films, and obtained thin-film devices consisting of electrodeposited Bi–Te and Sb–Te thin film legs. Later, they fabricated a device based on a new double-layer-leg thin-film concept by flip-chip bonding of 242 pairs of thin-film legs.[57] Using electrodeposition technique and a post-annealing process, the nanoinclusion γ-SbTe in Sb_2Te_3 film was achieved.[34] Although the electrodeposition process is simple, the influencing factors are quite complex. The performance of deposited film depends not only on the current, voltage, temperature, solvent, solution pH value and concentration, but also the solution ionic strength, electrode surface state and other factors. It is relatively difficult to control the composition and thickness of films, especially in the preparation of ideal and/or complex composition films.

3. Inorganic thermoelectric films

The most widely studied and developed thermoelectric thin-film materials are still inorganic semiconductors, from chalcogenides, such as Bi_2Te_3, for room-temperature applications, PbTe, suitable for medium-temperature applications, to silicides, like SiGe, optimal for high-temperature applications.[21,23] In recent years, due to the development of material system and the exploration of new synthesis and preparation technology, researches on skutterudite compounds, which has typical "electronic crystal-phonon glass" characteristics, quantum well, superlattice, and oxide thermoelectric materials have made a great breakthrough, which inspired researchers to explore high-performance TE materials. The crystal structure, physical properties, and TE performance of several representative inorganic film materials are discussed in this section.

3.1. Low-temperature thermoelectric films

3.1.1. $(Bi,Sb)_2(Te,Se)_3$ compounds

$(Bi,Sb)_2(Te,Se)_3$ solid solution material, a V–VI compound semiconductor, is one of the earliest and most mature TE materials. It has been recognized as the best room-temperature TE material with larger Seebeck coefficient and electrical conductivity and lower thermal conductivity.[58] Bismuth telluride (Bi_2Te_3) is one of the best commercial TE materials. Stacking along the c axis of the unit cell by van der Waals interactions, it crystallizes into a hexahedral layered structure with five atomic layers (Te_1–Bi–Te_2–Bi–Te_1).[59] As is depicted in Fig. 1, Te_1–Bi has a layer spacing of 0.174 nm, which is a combination of covalent bond and ion bond. The Te_2 atoms are covalently bonded to the surrounding six Bi atoms by sp^3d^2 hybrids with a layer spacing of 0.203 nm. The interlayer spacing between Te_1 and Te_1 is 0.260 nm, the combination of van der Waals forces. Accordingly, Bi_2Te_3 crystals are prone to dissociation between Te_1 and Te_1 atoms. However, it displays unique properties like high Seebeck coefficient ($\sim -220\ \mu V\cdot K^{-1}$), good electrical conductivity ($\sim 4\times10^4\ S\cdot m^{-1}$), low thermal conductivity ($\sim 1.5\ W\cdot m^{-1}\cdot K^{-1}$), and small band gap (0.14 eV) at room temperature. What is more, it exhibits a low melting temperature of 585 °C.[17,60] The effects of different fabrication techniques on the TE performance of $(Bi,Sb)_2(Te,Se)_3$ films are summarized in Table 1.

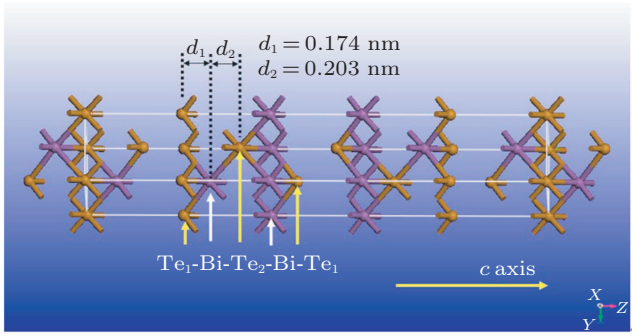


Fig. 1. (color online) The crystal structure of Bi_2Te_3.[59]

Taking advantage of low-dimensional structures and topological insulators, quintuple atomic layer films of Bi_2Te_3 and Sb_2Te_3 had been calculated in theory, showing high zT at room temperature, $zT = 7.15$ for Bi_2Te_3 quintuple atomic layer film, $zT \geq 2.1$ and $zT \geq 2.2$ for Sb_2Te_3 one and four quintuple layer films, respectively.[71,72] In addition, a zT value of ~2.4 had been obtained in experiment by preparing multiple-quantum-well Bi_2Te_3/Sb_2Te_3 superlattices.[20] Employing PLD technique, Bi_2Te_3 films with different morphologies at the micrometer/nanometer scale were deposited, and the zT was expected more than 1.5.[73] Zhang *et al.*[44] fabricated highly (00l)-oriented Bi_2Te_3 thin films with in-plane layered grown columnar nanostructure by a simple magnetron co-sputtering method. They demonstrated that this special nanostructure can not only achieve high power factor ($33.7\ \mu W\cdot cm^{-1}\cdot K^{-2}$) through unblocking electron transport, but also suppress the thermal conductivity ($0.86\ W\cdot m^{-1}\cdot K^{-1}$) due to phonon scattering by grain boundaries and interfaces. The n-type $Bi_2Te_{2.7}Se_{0.3}$ layered and columnar film with layered structure was achieved by simple magnetron co-sputtering method, and $zT = 1.27$ was obtained at room temperature.[65] Besides, a ternary compound n-type $Bi_2(Te,Se)_3$ film, which is depicted in Fig. 2, was prepared by thermal co-evaporation technique, and the room temperature zT of 1.01 was achieved.[27] Song *et al.*[66] fabricated p-type

Table 1. Effects of different fabrication techniques on the TE performance at room temperature of $(Bi,Sb)_2(Te,Se)_3$ films.

Film	Fabrication technique	$\sigma/10^4$ S·m^{-1}	S/μV·K^{-1}	$S^2\sigma/\mu$W·cm^{-1}·K^{-2}	k/W·m^{-1}·K^{-1}	zT	Ref.
Bi_2Te_3	MBE	10.04	−167	28	1.87	0.45	[61]
Bi_2Te_3	electrodeposition	1.59	−59.5	5.59	–	–	[57]
Sb_2Te_3	electrodeposition	0.28	441.2	54.8	–	–	[57]
Bi_2Te_3	thermal co-evaporation	7.94	−248	48.7	–	–	[62]
$Bi_2(Te,Se)_3$	thermal co-evaporation	4.9	−189	17.5	0.52	1.01	[27]
$Bi_{1.5}Sb_{0.5}Te_3$	thermal co-evaporation	7.6	226	38.0	0.91	1.28	[63]
Sb_2Te_3	magnetron co-sputtering	8.2	229	41.6	1.06	1.22	[64]
Bi_2Te_3	magnetron co-sputtering	8.4	−200	33.7	0.86	–	[44]
$Bi_2Te_{2.7}Se_{0.3}$	magnetron co-sputtering	6.9	−241	40.0	0.95	1.27	[65]
$Bi_{0.45}Sb_{1.55}Te_3$	magnetron co-sputtering	7.3	208	31.3	–	–	[66]
$Bi_{0.4}Sb_{1.6}Te_3$	flash evaporation + annealing	6.4	236	35.6	1.05	1.0	[38]
$Bi_{0.5}Sb_{1.5}Te_3$	DC magnetron sputtering + annealing	12.3	198	48.2	–	–	[67]
$Bi_{0.5}Sb_{1.5}Te_3$	magnetron sputtering	14.6	191.3	53.0	–	–	[68]
Sb_2Te_3	DC magnetron sputtering	2.8	136	5.2	0.37	0.42	[28]
Bi_2Te_3	screen printing + annealing	–	–	21.0	1.0	0.61	[69]
$Bi_2Te_{2.7}Se_{0.3}$	screen printing + annealing	4.77	190	–	0.65	0.90	[70]

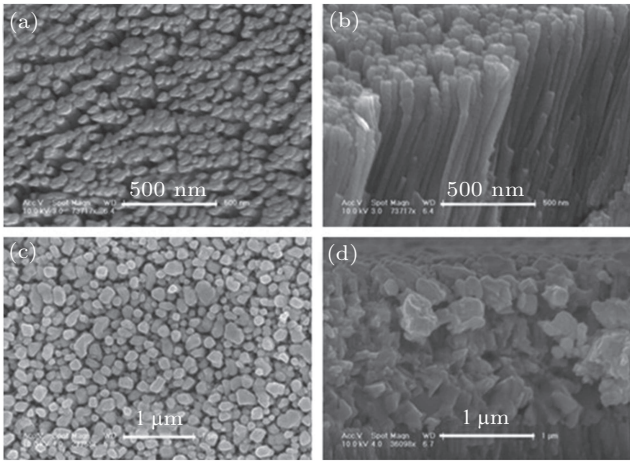


Fig. 2. (color online) SEM images of a ternary compound n-type $Bi_2(Te,Se)_3$ films [(a) and (b)] ordered nanowire array and [(c) and (d)] ordinary films with [(a) and (c)] surface view, (b) oblique view, and (d) cross-sectional view.[27]

$Bi_xSb_{2-x}Te_3$ thermoelectric thin films with various chemical compositions by a magnetron co-sputtering process. The largest power factor at room temperature reached 31.3 μW·cm^{-1}·K^{-2} for $Bi_{0.45}Sb_{1.55}Te_3$ film. The p-type (015)-preferential $Bi_{1.5}Sb_{0.5}Te_3$ multilayered film was deposited by a simple thermal co-evaporation technique, having a room-temperature zT of 1.28. And the in-plane transport mechanism was shown in Fig. 3.[63] Zhu *et al.*[67] achieved the preferential growth transformation from (015) plane to (00l) plane of $Bi_{0.5}Sb_{1.5}Te_3$ film by a facile post-annealing process, as illustrated in Fig. 4, and TE performance was enhanced. As a result, the power factor of (00l) preferential growth $Bi_{0.5}Sb_{1.5}Te_3$ film (48.2 μW·cm^{-1}·K^{-2}) is three times higher than that of the (015) preferential growth film. What is more, (00l)-orientation p-type Sb_2Te_3 and $Bi_{0.5}Sb_{1.5}Te_3$ also could be synthesized by sputtering method.[64,68] Shen *et al.*[28] directly deposited Sb_2Te_3 on flexible polyimide substrate, and obtained an Sb_2Te_3 thin film with (015) crystal preferential orientation, having a maximum power factor of 6.0 μW·cm^{-1}·K^{-2}. Byung Jin Cho *et al.*[69] printed Bi_2Te_3 thick film, and annealed at 500 °C in Bi and Te powders ambient, achieving a power factor of 21 μW·cm^{-1}·K^{-2}, a thermal conductivity of 1.0 W·m^{-1}·K^{-1}, and a zT value of 0.61 at room temperature. Using a post ionized defect engineering process, a maximum zT of 0.90 was obtained with the screen-printed n-type BiTeSe thick film at room temperature, which is almost comparable to that of the bulk $Bi_2Te_{2.7}Se_{0.3}$ and is a 2-fold increase over the same screen-printed film without the hydrogen ambient annealing.[70]

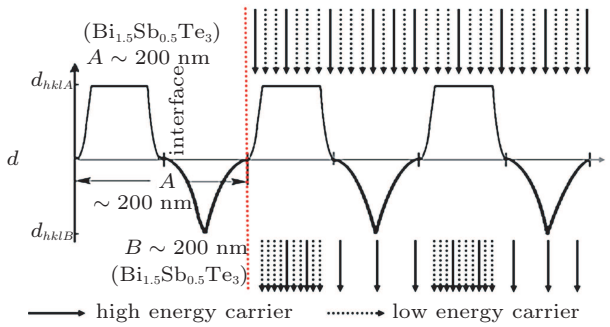


Fig. 3. (color online) The in-plane transport mechanism of the (015)-oriented $Bi_{1.5}Sb_{0.5}Te_3$ multilayered film with alternating stress field.[63]

3.1.2. Bismuth antimony ($Bi_{1-x}Sb_x$)

$Bi_{1-x}Sb_x$, an infinite solid solution with hexagonal structure, has been among the most attractive low-temperature TE materials for many decades, in virtue of their highly anisotropic transport properties, small effective mass and high mobility carriers. Because of its higher Seebeck coefficient

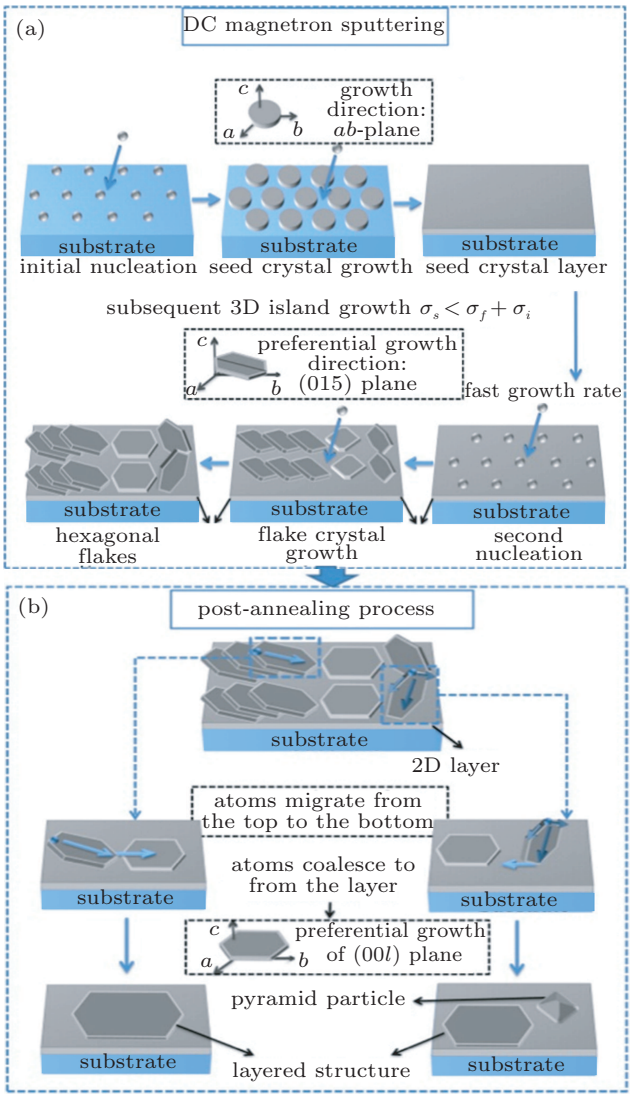


Fig. 4. (color online) (a) The growth mechanism of (015)-oriented $Bi_{0.5}Sb_{1.5}Te_3$ film; (b) the transformation mechanism of preferential growth from (015) plane to (00l) plane in $Bi_{0.5}Sb_{1.5}Te_3$ film.[67]

and lower thermal conductivity, the zT value of $Bi_{1-x}Sb_x$ is larger. As a result, it has been considered as one of the best n-type TE materials for cooling below room temperature. Feng *et al.*[35] reviewed that a maximum zT of ~0.42 for a $Bi_{1-x}Sb_x$ thin films was observed when $x = 0.18$ at 60 K in 2008. Later, Rogecheva *et al.*[74] in the year of 2011 synthesized the trigonal-orientated mosaic-single-crystal $Bi_{0.955}Sb_{0.045}$ films. Moreover, they found that the electrical conductivity and the Seebeck coefficient in the $Bi_{1-x}Sb_x$ films can be increased at the same time, which broke the negative correlation between electrical conductivity and Seebeck coefficient in other materials systems. Recently, nanostructured composites of $Bi_{1-x}Sb_x$ nanoparticles and carbon nanotubes had been prepared, and the study revealed that the TE properties of composites can be considerably improved compared to CNT free nanostructured $Bi_{1-x}Sb_x$.[75] Besides, there is a strong anisotropy of TE properties between along and perpendicular to the uniaxial pressing direction.

3.2. Medium-temperature thermoelectric films

3.2.1. Skutterudites

Skutterudite has drawn much attention in the last decade and it is expected to be a promising TE material owing to its high carrier concentration, excellent charge carrier mobility, good Seebeck coefficients, and (when suitably doped) a small thermal conductivity. Skutterudite refers to a material with a $CoAs_3$ type structure, exhibiting a distorted version of the MX_3-type perovskite structure (M = Rh, Co, Ir; X = Sb, P, As).[76] Skutterudite has a complex octahedral structure with two large voids in each cell, which is large enough to host large metal atoms to form filled skutterudites. The void-filling atom can act as an electron donor or electron acceptor, thus changing the electron concentration and electronic conductivity. Moreover, these void-filling atoms vibrate in the voids, causing a large scattering of phonons, and act as strong phonon scattering centers, which can reduce the lattice thermal conductivity. For instance, smaller and heavier atoms in the voids introduce significant disorder to the lattice, leading to a reduction in the lattice thermal conductivity.[11,76] Using Ba and Yb to fill the voids in $CoSb_3$, Shi *et al.*[77] obtained n-type double-filled skutterudites $Ba_xYb_yCo_4Sb_{12}$. Meanwhile, they revealed that the combination of Ba and Yb fillers inside the voids of the skutterudite structure provides a broad range of resonant phonon scattering and consequently a strong reduction in the lattice thermal conductivity, which results in a high zT of 1.36 at 800 K. 30-nm thick Co–Sb films were prepared by MBE though two different methods, and the TE properties were investigated.[78] They found that both films have bipolar conduction, which leads to poor power factors. What is more, by doping with Fe or Yb, they successfully produced p- and n-type doped samples and the larger power factors are obtained. Zheng *et al.*[79] fabricated Co-excess and Sb-excess $CoSb_3$ based thin films by RF and DC magnetron co-sputtering technique. They investigated that the thin film with excess Co exhibits a significant n-type conduction behavior and transforms to p-type conduction behavior with Sb rich, and the power factor of the Sb-excess sample has a high value of 6.9 $\mu W \cdot cm^{-1} \cdot K^{-2}$ which is ten times of the $CoSb_3$ thin film. Ahmed *et al.*[80] deposited $CoSb_3$ skutteruddite thin films by using RF co-sputtering method, and they reported a maximum power factor of 4.1 $\mu W \cdot cm^{-1} \cdot K^{-2}$ for the film deposited at a 200-°C substrate temperature. Recently, they synthesized a series of $CoSb_3$ thin films with Sb contents at room temperature via RF co-sputtering, and obtained a maximum power factor of 12.6 $\mu W \cdot cm^{-1} \cdot K^{-2}$[43] Using the deposition potential in electrochemical synthesis, Yadav *et al.*[81] exercise controlled the

structural and electrical properties, and associated tuning of TE properties of $CoSb_3$ thin films, and they achieved a highest roomtemperature power factor of 7.06 ± 0.09 $\mu W \cdot cm^{-1} \cdot K^{-2}$ at a deposition potential of -0.97 V.

3.2.2. Lead telluride (PbTe) and its derivatives

PbTe, a traditional TE material, crystallizes into the isomorphous cubic NaCl crystal structure with Pb atoms at the cationic sites and Te at the anionic sites, which can efficiently operate at medium temperatures owing to its high zT, excellent chemical stability, low vapor pressure, and high melting point (~900 K)[60,82] What is more, in virtue of its bandgap (~0.32 eV), PbTe can be doped into either n-type (Pb-rich PbTe) or p-type (Te-rich PbTe) TE material. In 2008, PbTe films of different thicknesses were deposited onto precleaned glass substrates under the pressure of 2×10^{-5} Torr by thermal evaporation.[83] Zhang *et al.*[82] prepared PbTe thin films on silicon substrates by an ALD for the first time, and they found that the formation of a PbTe thin film on the Si substrates was strongly dependent on the growth temperature. Samoilov and Dashevsky *et al.*[84,85] studied the indium-doped PbTe films and the influence of oxygen treatment on transport properties of PbTe:In polycrystalline films. Urban *et al.*[86] presented the first electronic measurements of multicomponent nanocrystal solids composed of PbTe and Ag_2Te in nature materials, which demonstrated synergistic effects can lead to enhanced p-type conductivity. $AgPb_mSbTe_{2+m}$ (LAST), a derivative of PbTe, has attracted much attention in recent years. LAST can be seen as the reaction between $AgSbTe_2$ and PbTe, resulting in the formation of $AgPb_mSbTe_{2+m}$ solid solution, the average structure of which is illustrated in Fig. 5.[87] In 2004, Hsu *et al.*[88] reported a zT value of 2.2 at 800 K in the quasi-binary system of the n-type $AgPb_mSbTe_{2+m}$. Last year, Hmood *et al.*[89] using solid-state microwave synthesis method prepared $AgPb_mSbTe_{2+m}$ compounds with different elements ratio of m ($0.0 \leq m \leq 10$), and the maximum power factor of 18.7 $\mu W \cdot cm^{-1} \cdot K^{-2}$ was obtained for the $AgPb_8SbTe_{10}$ sample resulting from a higher Seebeck coefficient. $AgPb_mSn_nSbTe_{2+m+n}$ (LASTT), developing with the addition of Sn atoms to LAST, has high performance of p-type TE properties, and could be considered as a p-type PbTe-based material for practical applications.[90] Ahn *et al.*[91] achieved a zT of ~1.1 at ~660 K for $Ag_{0.9}Pb_5Sn_5Sb_{0.8}Te_{12}$ mainly due to the very low lattice thermal conductivity of ~0.4 $W \cdot m^{-1} \cdot K^{-1}$ around 660 K. Another derivative of PbTe, $AgPb_mBiTe_{2+m}$ (BLST) has not yet been extensively studied, but its existence has been known for a long time. In 2016, Falkenbach *et al.*[92] reported the preparation and TE properties of nanostructured BLST, which achieved a high zT values close to the ones of bulk samples. However, few studies have focused on the TE properties of PbTe and its derivatives films.

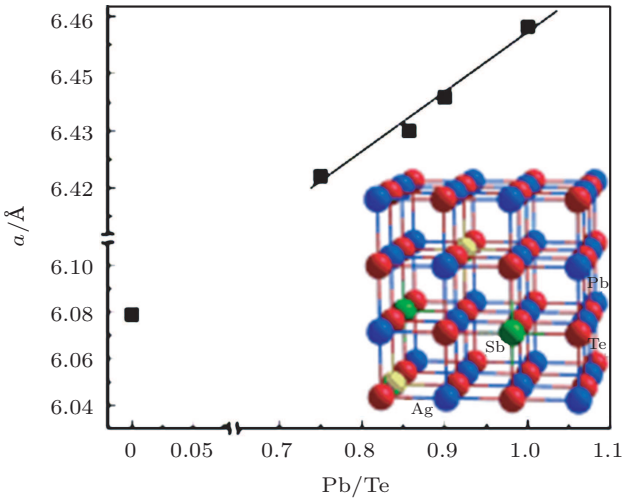


Fig. 5. (color online) Lattice parameters showing the LAST family follows Vegard's law, even though the system shows nanoscale phase segregation.[87]

3.3. High-temperature thermoelectric films

3.3.1. Silicon–germanium (Si–Ge) alloys

Si–Ge alloy, intermetallic compound, with high melting point, good mechanical properties, is a relatively mature high-temperature TE material. Furthermore, Si–Ge films are ideal candidates for many TE applications thanks to their low cost, low toxicity and high compatibility with microelectronics manufacturing. However, it has an obvious drawback of high thermal conductivities, impeding the improvement on zT. Many researchers have used calculation and simulation on thermal transport of different Si–Ge thin films, providing theoretical understanding of phonon scattering and its effect on thermal conductivity.[93–96] Iskandar *et al.*[95] solved the exact Boltzmann transport equation with spatial dependence of phonon distribution function. Moreover, considering the dispersion of confined phonon modes in nano-sized films, they deduced the thermal conductivity in single-crystal and polycrystalline Si–Ge thin-films, which help us to understand the interplay between phonons scattering within the boundaries and point-defects in Si–Ge thin-films in theory. Mascali[96] studied the effects of embedding nanoparticles in semiconductor alloy matrices especially $Si_{0.7}Ge_{0.3}$ alloy crystal through a new formula for thermal conductivity on basis of a hierarchy of hydrodynamical models, and they confirmed that the embedding nanoparticles can decrease the steady-state thermal conductivity. Experimentally, Lu *et al.*[53] synthesized high-performance p-type Si–Ge thin-films by LPCVD, and obtained a unique columnar grain structure, shown in Fig. 6, which influenced the films' thermal conductivity deeply. They emphasized that the energy barriers at grain boundaries play a crucial role in determining the charge transport properties which induced the big different influence of the columnar grain structure on in-plane and cross-plane thermal transport. Owning to the above theory, a high in-plane zT of 0.2 at room temperature has achieved by optimizing the growth conditions and

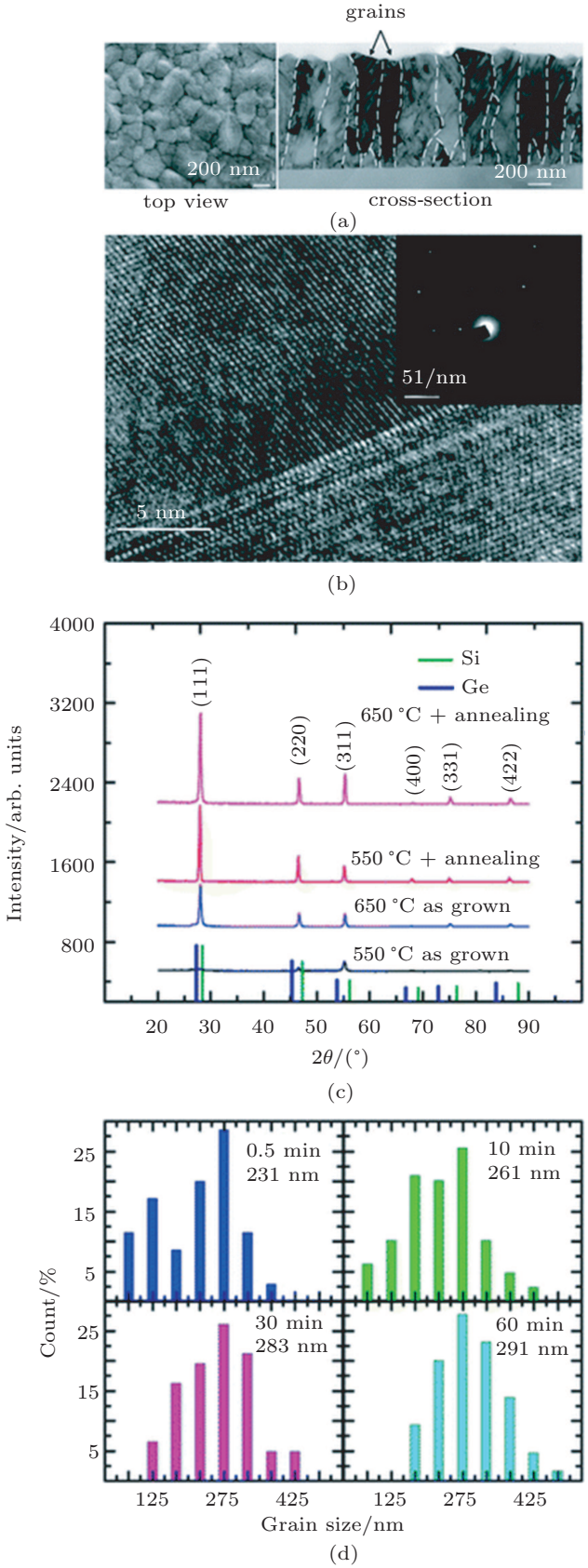


Fig. 6. (color online) (a) SEM of the top surface morphology and TEM of the cross-sectional structure of a polycrystalline Si–Ge thin-film grown by LPCVD at 650 °C; (b) High-resolution TEM of grains and grain boundaries. The inset picture shows the diffraction pattern of a grain; (c) X-ray diffraction (XRD) of Si–Ge thin-films. The vertical bars on the x axis indicate the corresponding patterns of Si and Ge single crystals; (d) The evolution of the grain size distribution of the Si–Ge thin-film with different annealing times, varying from 0.5 min to 60 min.[53]

boron doping level. What is more, they obtained phosphorus doped Si–Ge thin films by LPCVD and found that the segregation of phosphorus dopants plays a vital role in grain growth and TE transport properties.[97] Using the process of metal-induced crystallization (MIC), Lindorf *et al.*[98] fabricated thin films consisting of Si80Ge20/Al multilayers by sputter deposition and subsequent annealing on aluminum oxide substrates. They emphasized the ratio of Al to Si–Ge is very important and annealing can change transport property of the thin films. Efficient Si–Ge TE films had been successfully made by electrophoresis deposition, and the TE power factor of $Si_{0.8}Ge_{0.2}$ film is about 19 $\mu W{\cdot}cm^{-1}{\cdot}K^{-2}$, owing to the large carrier mobility.[99] Rowe *et al.*[100] showed a rapid method for producing thin films of free-standing B- and P-doped Si–Ge NCs by a nonthermal plasma and inertial impaction. Through DC sputtering, Perez-Taborda *et al.*[40] fabricated large area $Si_{0.8}Ge_{0.2}$ nano-meshed films with different porous sizes, and they found that the power factors are between 4.5 $\mu W{\cdot}cm^{-1}{\cdot}K^{-2}$ and 0.65 $\mu W{\cdot}cm^{-1}{\cdot}K^{-2}$. Furthermore, they used MIC to grow nanostructured $Si_{0.8}Ge_{0.2}$ films, and achieved a zT of 5.6×10^{-4} at room temperature with a relatively large power factor of 0.16 $\mu W{\cdot}cm^{-1}{\cdot}K^{-2}$.[101]

3.3.2. Half-Heusler compounds

As intermetallic compound, Half-Heusler (HH) alloy has chemical formula of ABX, where A is generally the most electropositive transition metal (e.g., Ti/Hf/Zr), B is a less electropositive transition metal (e.g., Co/Ni) and X is a main group element (e.g., Sb/Sn).[11,76] HH alloy has an MgAgAs-type cubic structure with three filled interpenetrating face-centered cubic (fcc) sublattices and one vacant fcc sublattice, possessing excellent mechanical and electrical properties, and good thermal stability.[11,102] Having relatively narrow bandgaps of 0.1 eV–0.3 eV, HH alloy exhibits high room-temperature Seebeck coefficients ($\sim$300 $\mu V{\cdot}K^{-1}$) and high room-temperature electrical conductivity ($\sim10^5$–10^6 $S{\cdot}m^{-1}$).[60] Zhu *et al.*[102] made intensive studies of HH alloy materials, particularly emphasized the TE transport features of n-type ZrNiSn-based HH alloys and p-type Fe (V, Nb) Sb-based HH compounds. What is more, they have reported p-type $FeNb_{1-x}Ti_xSb$ ($0.04\leq x\leq0.24$) with a zT of 1.1 at 1100 K and Hf dopant FeNbSb heavy-band HH alloys with a high zT of $\sim$1.5 at 1200 K.[103,104] Meanwhile, Wang *et al.*[105] deposited the HfNiSn thin-films by a custom-designed RF magnetron sputtering system, and investigated the effects of substrate temperature on the films' structure and TE property. They found the films have preferred-orientated (111) plan at substrate temperature of 400 °C, and TE properties of the orientated film exhibit anisotropic characteristics. And they obtained Seebeck coefficient of -68 $\mu V{\cdot}K^{-1}$ and power factor of 1.3 $\mu W{\cdot}cm^{-1}{\cdot}K^{-2}$ at room temperature. What else, p-type

semiconducting epitaxial NiYBi films were directly prepared on MgO (100) substrates by magnetron sputtering.[106] Kozina *et al.*[107] deposited multilayer stacks consisting of alternating NiTiSn and $NiZr_{0.5}Hf_{0.5}Sn$ layers by means of DC-sputtering. They achieved a high-quality crystalline structure by using NiTiSn as buffer layer for epitaxial growth of different thin-films and superlattices of both materials. Jaeger *et al.*[108] fabricated TiNiSn and $Zr_{0.5}Hf_{0.5}NiSn$ single crystalline thin-film by DC magnetron sputtering, and reported a power factor of 2.8 $\mu W\cdot cm^{-1}\cdot K^{-2}$ for $Zr_{0.5}Hf_{0.5}NiSn$ film at room temperature. Zhou *et al.*[109] synthesized n-type Zr–Ni–Sn thin-films with an amorphous microstructure by RF magnetron sputtering and achieved a Seebeck coefficient of -112.0 $\mu V\cdot K^{-1}$ and a power factor of 26.6 $\mu W\cdot cm^{-1}\cdot K^{-2}$ at 393 K when the sputtering power is 80 W.

3.3.3. Metal oxide

Metal oxide with high thermal stability, chemical stability, non-toxic, non-polluting, can be used in high temperature and atmospheric atmosphere, which has a broad application prospects as environment-friendly high-temperature TE materials. Layered cobaltites, including M_xCoO_2 (M = Na or Ca), $Ca_3Co_4O_9$, $Bi_2Sr_2Co_2O_y$, etc., are typical p-type oxide TE materials, which own higher conductivity and Seebeck coefficient, and lower thermal conductivity. Lee *et al.*[41] fabricated an Na_xCoO_2 thin film by an RF-magnetron sputtering method and found that the power factor (143 $\mu W\cdot cm^{-1}\cdot K^{-2}$) of the Na_xCoO_2 thin film is comparable to that of typical TE materials, such as Bi_2Te_3 cation-doped $(Ca_2CoO_3)_xCoO_2$ films were prepared by a metalorganic decomposition process.[110] Diao *et al.*[111] studied the TE properties of $Bi_2Sr_2Co_2O_y$ thin-film grown at different temperatures, and obtained a large power factor of 5.5 $\mu W\cdot cm^{-1}\cdot K^{-2}$ for the film grown at 700 °C. Furthermore, the transverse TE effect in c axis tilted $Bi_2Sr_2Co_2O_y$ thin-films has been investigated.[112] The current state-of-the-art n-type oxide TE material is represented by strontium titanates and doped zinc oxide. Using first-principles calculations, Zou *et al.*[113] made it clear to understand the nature of the anisotropic transport properties for $SrTiO_3$ under strain, and offered useful guidelines to design high performance $SrTiO_3$ thin-films. In addition, the zT for 20%-Nb-doped $SrTiO_3$ reached 0.35 at 1000 K.[114] The largest zT about 2.4 at 300 K has been estimated in a superlattice of $SrTiO_3$/ Nb:$SrTiO_3$[115] Using deionized water and ozone as oxidants, and diethylzinc as a zinc precursor, undoped ZnO thin-films have been deposited by ALD.[55] The schematic diagram is illustrated in Fig. 7.

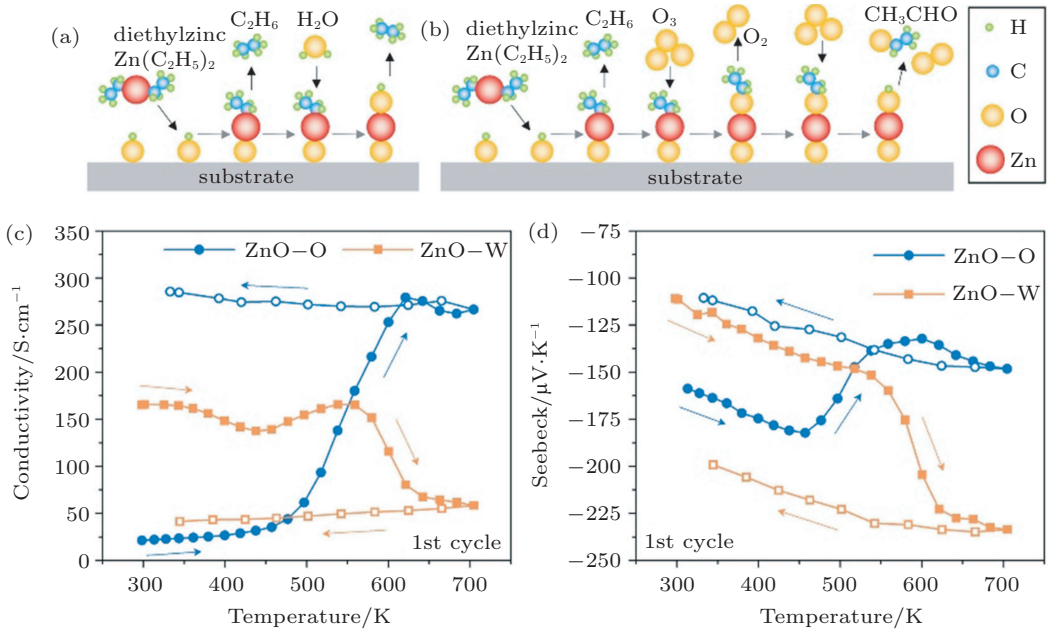


Fig. 7. (color online) Schematic illustration of the ALD mechanism for the growth process of (a) ZnO–W and (b) ZnO–O. All films were grown on a glass substrate, first, cycle temperature-dependent thermoelectric properties of ZnO–O and ZnO–W. (c) Electrical conductivity and (d) Seebeck coefficient. Drastically different properties of ZnO films are observed depending on the oxidant used (water versus ozone) during ZnO growth. Heating cycle and subsequent cooling cycle are presented with filled and open symbols, respectively.[55]

It was found that using the strong oxidant-ozone, undoped ZnO film could get a higher power factor of 5.76 $\mu W\cdot cm^{-1}\cdot K^{-2}$ than 2.89 $\mu W\cdot cm^{-1}\cdot K^{-2}$ for the water-based ZnO film. And the author deduced that the strong oxidant effect can explain those phenomena by a mechanism involving point defect-induced differences in carrier concentration between these two oxides and a self-compensation effect in water-based ZnO due to the competitive formations of both oxygen and zinc vacancies. Liu *et al.*[116] achieved a power factor of 3.198×10^{-4} $\mu W\cdot cm^{-1}\cdot K^{-2}$ at 210 °C for the film oxidized under 12-T condition, and confirmed that both Al dopant and application of high magnetic field can

be used to control structure and TE properties of doped ZnO films. Gallium-doped zinc oxide (GZO) thin-films were prepared by ALD.[117] The efficient Ga doping of GZO showed a Seebeck coefficient of 60 $\mu V \cdot K^{-1}$ and an electrical conductivity of 1.808×10^5 $S \cdot m^{-1}$, with a maximum power factor of 6.6 $\mu W \cdot cm^{-1} \cdot K^{-2}$. Furthermore, Nguyen *et al.*[118] investigated the effect of single Ga dopant (GZO) and dual Ga and In dopants (IGZO) on the TE properties of host ZnO films. They reported the zT of the pure ZnO, GZO, and IGZO thin films at 110 °C is 0.004, 0.012, and 0.019, respectively, and indicated that the balanced control of both electron and lattice thermal conductivities through dopant selection are necessary to attain low total thermal conductivity. Han *et al.* CdO with ZnO was successfully alloyed at a molar ratio of 1:9 which significantly reduced the thermal conductivity by up to 7-fold at room temperature.[119] They carefully selected the Sc-dopant concentrations, obtained a higher power factor of 7.1 $\mu W \cdot cm^{-1} \cdot K^{-2}$ at 1173 K, and achieved the highest zT ~0.3 at 1173 K for the $Zn_{0.9}Cd_{0.1}Sc_{0.01}O_{1.015}$ sample. Al_2O_3/ZnO thin films were deposited via ALD, and a zT value of 0.14 was obtained for the most efficient structure by manipulating them with a nano-thick Al_2O_3 interface.[120] Hoong *et al.*[121] successfully deposited Al_x-doped ZnO and $Zn_xFe_{3-x}O_4$ thin films onto glass substrates using inkjet printing with a minimum of 50 print cycles.

4. Organic and composite thermoelectric films

Compared with classic inorganic TE materials, organic TE materials are unique in flexibility, light weight, intrinsically low thermal conductivity, non-toxicity, inexpensiveness, rich resources, and easy of processing. Therefore, they can be used for low-temperature flexible TE devices. Among organic TE materials, the conductive polymers such as polyaniline (PANI), polyacetylene (PA), polypyrrole (PPy), polythiophene (PTh), poly(3,4-ethylenedioxythiophene) (PEDOT), poly(3,4-ethylenedioxythiophene): poly(styrenesulfonate) (PEDOT:PSS), and their nanocomposites have sparked intense interest and gained remarkable achievements.[21,60,122,123] Conductive polymers have intrinsically low thermal conductivity, about 1–3 orders of magnitude lower than that of inorganics, broad range of electrical conductivity from 10^{-6} $S \cdot m^{-1}$ to 10^6 $S \cdot m^{-1}$, and the Seebeck coefficient of 10 $\mu V \cdot K^{-1}$~103 $\mu V \cdot K^{-1}$.[122] What is more, like the inorganic TE materials, they also have the general trade-off relationship between electrical conductivity and Seebeck coefficient.[123] Many researchers have focused on enhancement of organic TE materials by control the oxidation level, doping, crystallinity, and nanocomposite, and so on.[124–126] The TE properties of typical conductive polymer TE films are briefly discussed in this section.

4.1. PANI-based thermoelectric films

PANI is a promising candidate for use in next-generation TE devices owing to its relatively low cost, easy processing, and environmental stability. Furthermore, the electronic conductivity of PANI is easy to control (e.g., ease of reversible conversion from an insulating into a conducting state) by the processing conditions and the disorder degree in the structure.[60,127] Figure 8 shows the chemical structure of PANI, in which y expresses the oxidation level and the three different structures: $y = 1$ (leucoemeraldine), $y = 0.5$ (emeraldine), and $y = 0$ (pernigraniline).

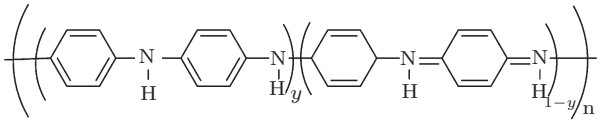


Fig. 8. Chemical structure of PANI.

However, PANI has a very poor TE response, because of its relatively low electrical conductivity and low Seebeck coefficient. Until now, almost all the reported power factors of pure PANI are no more than the order of 10^{-8} $\mu W \cdot cm^{-1} \cdot K^{-2}$, which is about 2~3 orders of magnitude less than those of inorganic TE materials.[127] The electrical conductivity of PANI is deeply affected by molecular arrangement, interchain separation, oxidation level, crystallinity, and doping. So far, many researchers have tried to increase the electrical conductivity and Seebeck coefficient of PANI. Li *et al.*[128] prepared HCl-doped PANI by chemical oxidative polymerization, and they found that electronic conductivity and zT increase with increasing HCl concentration, but the Seebeck coefficient decrease. For 1-M HCl-doped PANI, they achieved the maximum zT of 2.67×10^{-4} at 423 K. Sun *et al.*[129] fabricated β-naphthalene sulfonic acid-doped PANI nanotubes with larger Seebeck coefficient of 212.4 $\mu V \cdot K^{-1}$, lower electronic conductivity (0.77 $S \cdot m^{-1}$) and thermal conductivity (0.21 $W \cdot m^{-1} \cdot K^{-1}$). They demonstrated that tubular nanostructures are effective for improving TE properties. Wang *et al.*[127] used self-assembled supramolecule (SAS) (3,6-dioctyldecyloxy-1,4-benzenedicarboxylic acid) as an additive and introduced into PANI films. They concluded that the addition of SAS greatly enhanced the TE power factor, maximum at 0.31 $\mu W \cdot cm^{-1} \cdot K^{-2}$. Yang *et al.*[130] synthesized PANI films by pulse electrodeposition method in different acidic solutions. By integrating high Seebeck coefficient tellurium nanorods with the conducting polymer PANI, Wang *et al.*[131] prepared a high-performance PANI/Te hybrid films, illustrated in Fig. 9, which were realized by carefully control of the polymer conformation and interfaces between PANI and Te nanorods. They found that the ordered conformation of the PANI chains surrounding the Te nanorods increased the carrier scattering and provided a high-speed carrier moving channel

resulting in an enhanced electronic conductivity. Moreover, the well-matched nanoscale interfaces improved carrier transport properties yet keep the thermal conductivity at a rather low level of 0.2 $W{\cdot}m^{-1}{\cdot}K^{-1}$. Based on the above simultaneous optimization, they achieved a maximum zT of 0.156 at room temperature and 0.223 at 390 K.

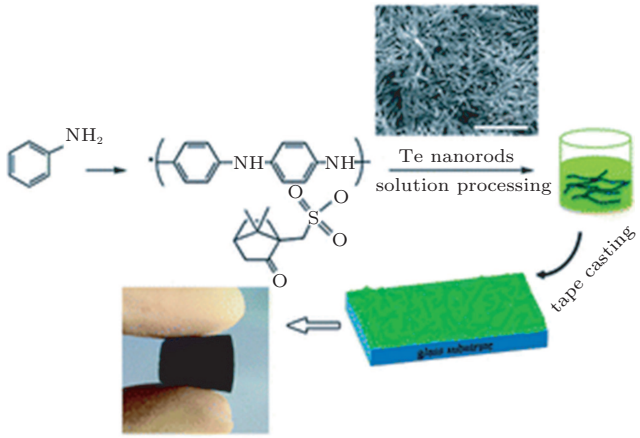


Fig. 9. (color online) Illustration of PANI/Te hybrid film processing with the embedded pictures showing the morphologies of Te nanorods and the hybrid film with a Te content of 60 wt%.[131]

4.2. PPy-based thermoelectric films

PPy, an electroactive polymer, has ignited great interest as a promising TE candidate due to its good electrical conductivity with relatively low thermal conductivity, facile synthesis, no toxicity, compositional flexibility, and good mechanical property. It is relatively stable and easy to fabricate by chemical or electrochemical polymerization. Wu *et al.*[132] fabricated two flexible and free-standing PPy nanotube films (PPy-1 and PPy-2), and obtained a maximum zT of 7.84×10^{-4} at 370 K for PPy-2 film. Besides, they concluded that the smaller size and longer length of PPy nanotubes are helpful to enhance the electrical conductivity and Seebeck coefficient but basically not affect thermal conductivity. An ultrathin PPy film was prepared by an electrochemical method in a cell of three electrodes.[133] Moreover, controlling the applied voltage, a highest zT of 6.8×10^{-3} was achieved. Li *et al.*[134] studied the electrical transport properties of p-type crystalline and amorphous PPy through first-principles and the thermal transport properties by molecular dynamics simulations. For hexafluorophosphate doped PPy, they confirmed that the crystalline phase leads to extra high electrical conductivity, and the amorphous phase possesses high Seebeck coefficient and low thermal conductivity. Besides, they deduced the zT along the chain direction of crystalline phase is higher than that of the amorphous phase. Using a common vacuum filtration method, Liang *et al.*[135] prepared a super flexible polypyrrole/single-walled carbon nanotube composites, and they found that there is no obvious deterioration of TE performance after mechanical bending or stretching.

4.3. PEDOT-based thermoelectric films

PEDOT, a prominent and extensively explored conducting polymer system, has been studied as a leading organic TE material due to its low thermal conductivity, low density, solution processability, and environmental stability. Figure 10 depicts the chemical structure of PEDOT, which has a simple electronic band structure with a bandgap of 0.9 eV. Furthermore, the p-type and n-type PEDOT possess higher Seebeck coefficient of about 100 $\mu V{\cdot}K^{-1}$ and 140 $\mu V{\cdot}K^{-1}$, respectively. But it has relatively low electronic conductivity, which limits its using in TE devices.[60,136]

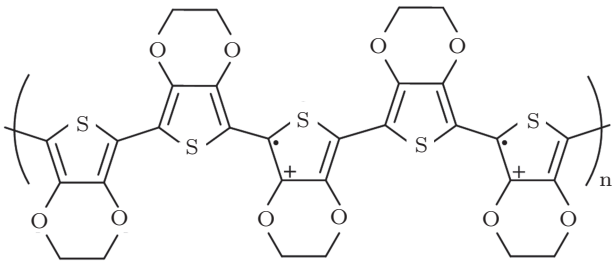


Fig. 10. Chemical structure of PEDOT.

As is known, incorporating conductive species can increase the electrical conductivity of electronically conductive polymers. Bubnova *et al.*[137] polymerized PEDOT: tosylate (PEDOT: Tos) by directly mixing the EDOT monomers and an oxidative solution of iron (III) tris-p-toluenesulfonate, and obtained a zT of 0.25 at room temperature. They found that accompanied with the interaction between the adjacent polymer chains and the Tos counterions on the outside of the chain stacks, the electronic conductivity of PEDOT: Tos is enhanced. Khan *et al.*[138] studied the effect of pH on TE property of PEDOT: Tos films by simply using acid (HCl) or base (NaOH) aqueous solutions. The pH treating lead to different oxidation level of PEDOT: Tos films and the maximum PF of 0.26 $\mu W{\cdot}cm^{-1}{\cdot}K^{-2}$ was achieved at pH $\leq$ 7.

The addition of poly(styrenesulfonate) (PSS) into PEDOT have been reported to enhance the electronic conductivity, resulting in an increase in electronic conductivity of about 9% compared with PEDOT: Tos. Recently, most studies on PEDOT: PSS films have focused on the improvement of electrical conductivity. Shi *et al.*[124] concluded different physical and chemical approaches which can effectively improve the electronic conductivity of PEDOT: PSS, and summarized the electronic conductivity enhanced mechanism in detail. Adding solid chloroplatinic acid (H_2PtCl_6) into the pristine PEDOT: PSS solution, Wu *et al.*[139] enhanced the electrical conductivity of PEDOT: PSS films by three orders of magnitude to 1.094×10^5 $S{\cdot}m^{-1}$. They concluded that compared with polar organic solvents, solid acid like H_2PtCl_6 is more effective to enhance the electrical conductivity of PEDOT: PSS films. Besides, they deduced the mechanism is attributed to PEDOT doping by Pt ions, phase segregation of

PSS chains from PEDOT: PSS, and the conformational change of PEDOT chains. Yi *et al.*[140] enhanced TE properties of PEDOT: PSS films through binary secondary dopants, dimethyl sulfoxide (DMSO) and poly(ethylene oxide) (PEO). They emphasized the binary secondary dopants both increased electrical conductivities and Seebeck coefficients. Kim *et al.*[141] proposed a solution treatment to promote crystal formation in PEDOT: PSS through a structural rearrangement process by H_2SO_4 post-treatment. In this case, electronic conductivity increased with the improvement in crystallinity, and achieved the highest value of 4.38×10^5 S·m^{-1}. As shown in Fig. 11, they viewed that structural rearrangement formed highly ordered and densely packed PEDOT: PSS nanofibrils, which improved both carrier concentration and mobility, resulting in an increased electronic conductivity. More recently, Fan *et al.*[142] enhanced TE properties of PEDOT: PSS films by sequential post-treatments with common acids and bases. Zhang *et al.*[143] significantly enhanced the electrical conductivity of PEDOT: PSS from 30 S·m^{-1} up to higher than 10^5 S·m^{-1} by treated with water-soluble vitamin B3. In addition, Beretta *et al.*[144] studied the TE properties of inkjet-printed commercially available PEDOT: PSS films in detail and achieved the in-plane zT no less than $\sim 10^{-3}$.

Using layer-by-layer assembly technique, Cho *et al.*[145] fabricated a completely carbon-based polymer nanocomposite by alternately depositing PANI, PEDOT: PSS-stabilized graphene, and stabilized double-walled nanotube (DWNT) from aqueous solutions, which is illustrated in Fig. 12. This quad-layer film obtained a higher roomtemperature power factor of 27.1 μW·cm^{-1}·K^{-2}, which can be compared with commercially available bismuth telluride. Jiang *et al.*[146] prepared PANI/PEDOT/PSS composite films and investigated the solvent effects of deionized H_2O and $NH_3 \cdot H_2O$ on electrical conductivity and Seebeck coefficient of the composite films. They obtained a maximum electrical conductivity

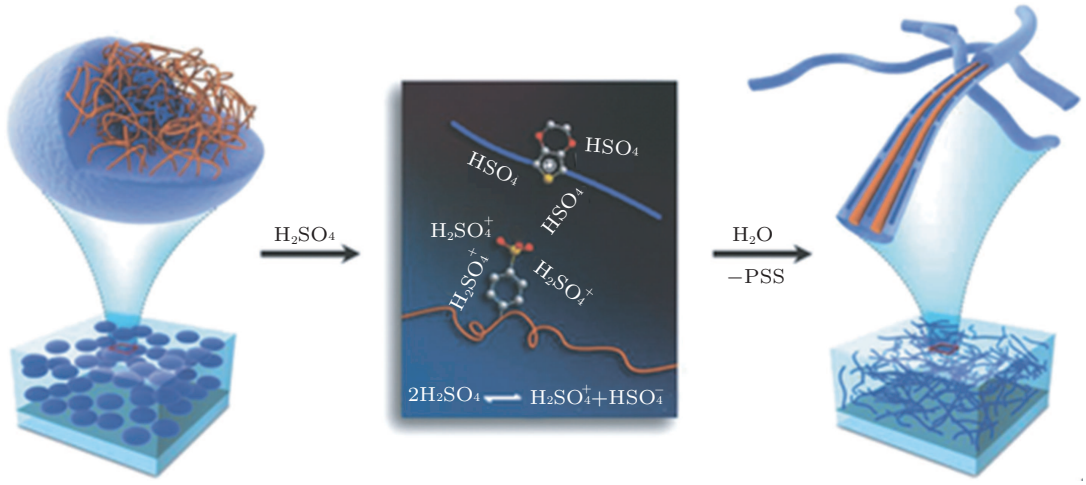


Fig. 11. (color online) Diagram of the structural rearrangement of PEDOT:PSS. The amorphous PEDOT:PSS grains (left) are reformed into crystalline PEDOT:PSS nanofibrils (right) via a charge-separated transition mechanism (middle) via a concentrated H_2SO_4 treatment.[141]

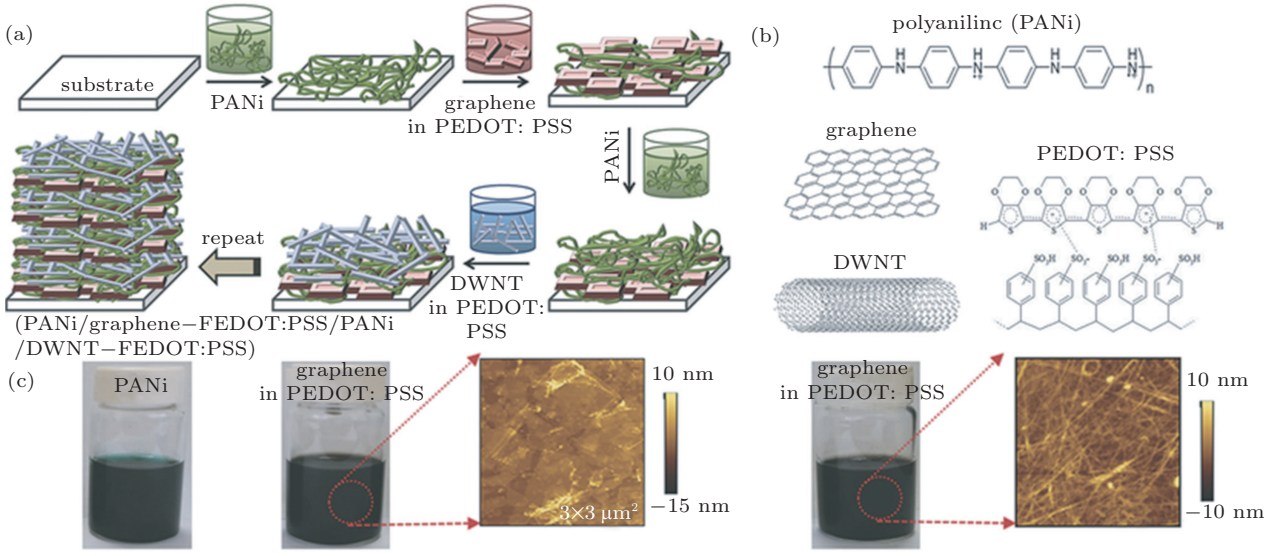


Fig. 12. (color online) (a) Schematic view of the layer-by-layer deposition process; (b) The structure of TE film components used; (c) Images of aqueous PANI solution, graphene and DWNT stabilized by PEDOT: PSS, in water. AFM topographical images of the corresponding suspensions cast onto silicon wafers are shown next to graphene and DWNT suspensions.[145]

(6.35×10^3 S·m^{-1}) of the composite film, which is much higher than pure PANI and pristine PEDOT/PSS. A flexible and freestanding PEDOT: PSS/PVA/BST (PPBST) nanocomposite TE films were fabricated by the blend of conductive polymer PEDOT: PSS, plastic reinforcer polyvinyl alcohol (PVA), and inorganic $Bi_{0.5}Sb_{1.5}Te_3$ (BST) TE nanocrystals, in addition, a power factor of 0.477 μW·cm^{-1}·K^{-2} and a zT value of 0.05 were achieved at 300 K.[147] Using facile direct vacuum filtration method, Jiang *et al.*[148] made PEDOT:PSS/MoS_2 (PM) thin-films through simply added a small amount of liquid-phase exfoliated MoS_2 nanosheets into PEDOT:PSS solutions, and achieved an optimized power factor of 0.456 μW·cm^{-1}·K^{-2} for the PM film with 4-wt% MoS_2 exfoliated in DMF. They found that the addition of MoS_2 nanosheets not only enhanced the electrical conductivity (1.25×10^5 S·m^{-1}) dramatically, owing to organic solvents effectively removal some PSS during the film formation, but also slightly increase the Seebeck coefficient from 14.5 to 19.5 μV·K^{-1}.

5. Strategies to enhance the thermoelectric performance of films

Compared with bulks, the TE films possess its unique features in electric and thermal conductivity mechanism. In a recent report by Zhou,[149] bulk materials with two-dimensional (2D) structures show outstanding properties, and their high performance originates from both their low thermal conductivity and high Seebeck coefficient due to their strong anisotropic features. As for low-dimensional TE thin films, it is much easier to own natural anisotropy and tailor electrical transport and thermal transport compared to TE bulks. On the other hand, the thermal conductivity can be largely reduced by phonon scattering at film boundary, grain boundary and interface without reducing the electrical conductivity.[17,18] In particular, the phonon-boundary scattering is of vital important for low-dimensional TE films.

Thanks to low-dimensional and unique structural characteristics of films, higher zT may be obtained in well-controlled TE films. In 2001, Venkatasubramaniam *et al.*[20] synthesized multiple-quantum-well Bi_2Te_3/Sb_2Te_3 superlattices and a highest zT value of ∼2.4 was achieved, which was attributed to the reduced thermal conductivity of 0.4 W·m^{-1}·K^{-1}–0.6 W·m^{-1}·K^{-1} by controlling the transport of phonons and electrons without any effect on the power factor. The core idea of enhancing the TE properties of films is to optimize the electron band structure by tuning the band filling to attain an optimal carrier concentration and improve the electronic DOS near Fermi level to optimize the power factor. At the same time, the thermal conductivity is reduced due to more phonon scattering centers without reducing the electrical conductivity, contributing an increase in zT. In recent years, lots of strategies and concepts have been developed to enhance the electrical and thermal transport in films, including modulation doping, energy filtering, and band convergence.[12,13,26,37,39,150–152]

However, the interrelated relationship among TE parameters obstructs the improvement of TE performance, such as σ and S having an inverse relationship with the carrier concentration (n), the effective mass (m^*), and the carrier mobility (μ) making another mutually counter-indicated relations. For the sake of getting the maximum available zT and exploiting the full potential of a given TE material, Zhu *et al.*[2] advanced that these advantageous strategies must be integrated to decouple electrical and thermal transport to optimize TE properties synergistically in the context of deep understanding of the underlying transport phenomena. Lee *et al.*[153] demonstrated a negative correlation between electrical conductivity and thermal conductivity in 2D SnS_2 nanosheets, which is beneficial for zT enhancement to reach above 3 at high temperatures (900 K).

Additionally, great efforts have been made to optimize the TE properties of films by controlling its microstructure and oriented growth.[44,65,73,154] Deng *et al.*[155] reported that the Bi_2Te_3-based TE film with preferential growth of (00l) plane facilitates the optimization of TE performance, because the (00l)-orientation is in favor of growth of layered structure and the enhancement of carrier mobility and electron scattering parameter of films. The maximum power factor value of 38 μW·cm^{-1}·K^{-2} has been achieved at 360 K. What is more, this special column structure with layered nanostructure in each column scatters more phonon at the increased grain boundaries and thus decreases the thermal conductivity. Zhu *et al.*[67] also enhanced the TE performance of $Bi_{0.5}Sb_{1.5}Te_3$ film about three times by transforming the film from (015)-orientation to (00l)-orientation using a facile post-annealing process.

6. Summary and outlook

TE materials have attracted extensive interest for their environmentally friendly in power generation and refrigeration, providing solutions to solve the energy crisis and pollution. TE materials in 2D film structures have potential applications in microdevices, which is in line with ongoing miniaturization of electronic circuits. Nowadays, most TE films are inorganic semiconductors like Bi_2Te_3, PbTe, Si–Ge, due to their excellent TE properties. The emerging organic TE materials, such as PEDOT, PANI, PPy, and their composites have also drawn the eyes of many researchers. To explore high-performance TE films, many methods for film manufacture have been developed, such as vacuum evaporation, sputtering, screen printing, MBE, ALD, and the like. Great efforts have been made to optimize the electrical and thermal properties in films, including tuning the carrier concentration, engineering

the band structure, and suppressing the lattice thermal conductivity. All in all, some significant advances in TE films have been achieved in the last few years. However, how to synergistically control the electrical and thermal transport in TE films is still challenging. Engineering the well-controlled nanostructures in TE films to create some sort of channels for the easy transmission of electrons but blocking the transmission of phonons would probably become an effective regulation direction in the future.

References

[1] He J and Tritt T M 2017 *Science* **357** 1369
[2] Zhu T, Liu Y, Fu C, Heremans J P, Snyder J G and Zhao X 2017 *Adv. Mater.* **29** 1605884
[3] Dong P, Rodrigues M F, Zhang J, Borges R S, Kalaga K, Reddy A L M, Silva G G, Ajayan P M and Lou J 2017 *Nano Energy* **42** 181
[4] Zhu W, Deng Y and Cao L 2017 *Nano Energy* **34** 463
[5] Shi X and Chen L 2016 *Nat. Mater.* **15** 691
[6] Zhang T, Li K, Zhang J, Chen M, Wang Z, Ma S, Zhang N and Wei L 2017 *Nano Energy* **41** 35
[7] Wang W, Jia F, Huang Q and Zhang J 2005 *Microelectron. Eng.* **77** 223
[8] Da Silva L W and Kaviany M 2004 *Int. J. Heat Mass Transfer* **47** 2417
[9] Tan G, Zhao L and Kanatzidis M G 2016 *Chem. Rev.* **116** 12123
[10] Hicks L D and Dresselhaus M S 1993 *Phys. Rev. B* **47** 12727
[11] Fitriani, Ovik R, Long B D, Barma M C, Riaz M, Sabri M F M, Said S M and Saidur R 2016 *Renw. Sust. Energ. Rev.* **64** 635
[12] Szczech J R, Higgins J M and Jin S 2011 *J. Mater. Chem.* **21** 4037
[13] Vineis C J, Shakouri A, Majumdar A and Kanatzidis M G 2010 *Adv. Mater.* **22** 3970
[14] Humphrey T E and Linke H 2005 *Phys. Rev. Lett.* **94** 96601
[15] Ohta H, Kim S, Mune Y, Mizoguchi T, Nomura K, Ohta S, Nomura T, Nakanishi Y, Ikuhara Y, Hirano M, Hosono H and Koumoto K 2007 *Nat. Mater.* **6** 129
[16] Ohta H 2008 *Phys. Status Solidi B* **245** 2363
[17] Rowe D M 2006 *Thermoelectrics Handbook* (Boca Raton London/New York: CRC Press Taylor & Francis Group) p. 253
[18] Chen G 2001 *Phonon transport in low-dimensional structures* (San Diego: Elsevier Academic Press INC) pp. 203–259
[19] Koga T, Sun X, Cronin S B and Dresselhaus M S 1998 *Appl. Phys. Lett.* **73** 2950
[20] Venkatasubramanian R, Siivola E, Colpitts T and O'Quinn B 2001 *Nature* **413** 597
[21] Caballero-Calero O and D'Agosta R 2017 *ECS J. Solid State Sci. Technol.* **6** N3065
[22] Eslamian M 2017 *Nano-Micro. Lett.* **9** 3
[23] Zhang X and Zhao L 2015 *Journal of Materiomics* **1** 92
[24] Peng S, Wang D, Lu J, He M and Xu C 2017 *J. Polym. Environ.* **25** 1208
[25] Liang Z, Boland M J, Butrouna K, Strachan D R and Graham K R 2017 *J. Mater. Chem. A* **5** 15891
[26] Wan C, Tian R, Kondou M, Yang R and Zong P 2017 *Nat. Commun.* **8** 1024
[27] Tan M, Deng Y and Wang Y 2014 *Nano Energy* **3** 144
[28] Shen S, Zhu W, Deng Y, Zhao H, Peng Y and Wang C 2017 *Appl. Surf. Sci.* **414** 197
[29] Kong X, Zhu W, Cao L, Peng Y, Shen S and Deng Y 2017 *ACS Appl. Mater. Inter.* **9** 25606
[30] Cam Tuyen L T, Le P H, Luo C W and Leu J 2016 *J. Alloys Compd.* **673** 107
[31] Kim S J, We J H and Cho B J 2014 *Energy Environ. Sci.* **7** 1959
[32] Zhang K, Yadav A, Shao L, Bommena R, Zhao J, Velicu S and Pipe K P 2016 *AIP Adv.* **6** 75009
[33] Park N, Ahn J, Park T, Lee J, Lee W, Cho K, Yoon Y, Choi C, Park J and Lee S 2017 *Nanoscale* **9** 7027
[34] Kim J, Zhang M, Bosze W, Park S, Lim J and Myung N V 2015 *Nano Energy* **13** 727
[35] Feng X, Hangarter C, Yoo B, Rheem Y and Lee K H 2008 *Electrochim. Acta* **53** 8103
[36] Chowdhury I, Prasher R, Lofgreen K, Chrysler G, Narasimhan S, Mahajan R, Koester D, Alley R and Venkatasubramanian R 2009 *Nat. Nanotechnol.* **4** 235
[37] Termentzidis K, Pokropyvnyy O, Woda M, Xiong S and Chumakov Y 2013 *J. Appl. Phys.* **113** 13506
[38] Takashiri M, Tanaka S and Miyazaki K 2010 *Thin Solid Films* **519** 619
[39] Xu S, Zhu W, Zhao H, Xu L, Sheng P, Zhao G and Deng Y 2018 *J. Alloys Compd.* **737** 167
[40] Perez-Taborda J A, Mu? noz Rojo M, Maiz J, Neophytou N and Martin- Gonzalez M 2016 *Sci. Rep.* **6** 32778
[41] Lee H S, Kim G H, Hwang D H and Woo S I 2015 *Curr. Appl. Phys.* **15** 412
[42] Hong J, Lee S and Yoon S 2014 *J. Alloys Compd.* **583** 111
[43] Ahmed A and Han S 2017 *Appl. Surf. Sci.* **408** 88
[44] Zhang Z, Wang Y, Deng Y and Xu Y 2011 *Solid State Commun.* **151** 1520
[45] Pelenovich V O, Xiao R, Liu Y, Liu P, Li M, He Y and Fu D 2015 *Thin Solid Films* **577** 119
[46] Yoo T, Lee E, Dong S, Li X, Liu X, Furdyna J K, Dobrowolska M and Luo T 2017 *APL Mater.* **5** 66101
[47] Wang Z, Zhang X, Wu Y and Hu Z 2015 *J. Electron. Mater.* **44** 3334
[48] Jiang Y, Sun Y Y, Chen M, Wang Y and Li Z 2012 *Phys. Rev. Lett.* **108** 66809
[49] Apreutesei M, Debord R, Bouras M, Regreny P, Botella C, Benamrouche A, Carretero-Genevrier A, Gazquez J, Grenet G, Pailhes S, Saint-Girons G and Bachelet R 2017 *Sci. Technol. Adv. Mat.* **18** 430
[50] Shin S, Kumar R, Roh J W, Ko D S and Kim H S 2017 *Sci. Rep.* **7** 7317
[51] Lu Z, Layani M, Zhao X, Tan L P, Sun T, Fan S, Yan Q, Magdassi S and Hng H H 2014 *Small* **10** 3551
[52] Madan D, Wang Z, Wright P K and Evans J W 2015 *Appl. Energy* **156** 587
[53] Lu J, Guo R, Daia W and Huang B 2015 *Nanoscale* **7** 7331
[54] Mahmood K, Alia A, Arshad M I, Nabi M A U, Amin N, Murtaza S F, Rabia S and Khan M A 2017 *J. Exp. Theor. Phys.* **124** 580
[55] Kim H, Wang Z, Hedhili M N, Wehbe N and Alshareef H N 2017 *Chem. Mater.* **29** 2794
[56] Kim M and Oh T 2011 *J. Electron. Mater.* **40** 759
[57] Kim M and Oh T 2014 *J. Electron. Mater.* **43** 1933
[58] Poudel B, Hao Q, Ma Y, Lan Y, Minnich A, Yu B, Yan X, Wang D, Muto A, Vashaee D, Chen X, Liu J, Dresselhaus M S, Chen G and Ren Z 2008 *Science* **320** 634
[59] Xie W, Tang X, Yan Y, Zhang Q and Tritt T M 2009 *J. Appl. Phys.* **105** 113713
[60] Gayner C and Kar K K 2016 *Prog. Mater. Sci.* **83** 330
[61] Peranio N, Eibl O and Nurnus J 2006 *J. Appl. Phys.* **100** 114306
[62] Goncalves L M, Couto C, Alpuim P, Rolo A G, Völklein F and Correia J H 2010 *Thin Solid Films* **518** 2816
[63] Tan M, Deng Y and Hao Y 2013 *Phys. Status Solidi A* **210** 2611
[64] Tan M, Deng Y and Hao Y 2013 *Chem. Phys. Lett.* **584** 159
[65] Tan M, Deng Y and Hao Y 2014 *Mater. Chem. Phys.* **146** 153
[66] Song J, Yao Q, Wu T, Shi X and Chen L 2013 *Electron. Mater. Lett.* **9** 709
[67] Zhu W, Deng Y, Wang Y, Luo B and Cao L 2014 *Thin Solid Films* **556** 270
[68] Cao L, Wang Y, Deng Y, Gao H, Luo B and Zhu W 2013 *J. Nanopart. Res.* **15** 8
[69] We J H, Kim S J, Kim G S and Cho B J 2013 *J. Alloys Compd.* **552** 107
[70] Kim S J, Choi H, Kim Y, We J H, Shin J S, Lee H E, Oh M, Lee K J and Cho B J 2017 *Nano Energy* **31** 258
[71] Zahid F and Lake R 2010 *Appl. Phys. Lett.* **97** 212102
[72] Li Z, Miao N, Zhou J, Sun Z, Liu Z and Xu H 2018 *Nano Energy* **43** 285
[73] Li Bassi A, Bailini A, Casari C S, Donati F, Mantegazza A, Passoni M, Russo V and Bottani C E 2009 *J. Appl. Phys.* **105** 124307
[74] Tang S and Dresselhaus M S 2014 *J. Mater. Chem. C* **2** 4710
[75] Günes E, Gundlach F, Elm M T, Klar P J, Schlecht S, Wickleder M S and Müller E 2017 *ACS Appl. Mater. Inter.* **9** 44756
[76] Liu W, Yan X, Chen G and Ren Z 2011 *Nano Energy* **1** 42
[77] Shi X, Kong H, Li C P, Uher C and Yang J 2008 *Appl. Phys. Lett.* **92** 182101
[78] Daniel M V, Lindorf M and Albrecht M 2016 *J. Appl. Phys.* **120** 125306
[79] Zheng Z, Li F, Li F, Li Y, Fan P, Luo J, Liang G, Fan B and Zhong A 2017 *Thin Solid Films* **632** 88

[80] Ahmed A and Han S 2014 *J. Korean Phys. Soc.* **65** 1614
[81] Yadav S, Yadav B S, Chaudhary S and Pandya D K 2017 *RSC Adv.* **7** 20336
[82] Zhang K, Pillai A, Tangirala M, Nminibapiel D and Bollenbach K 2014 *Phys. Status Solidi A* **211** 1329
[83] Kungumadevi L, Rajasekar K, Subbarayan A and Sathyamoorthy R 2008 *Ionics* **14** 63
[84] Samoilov A M, Buchnev S A, Dolgopolova E A, Synorov Y V and Khoviv A M 2004 *Inorg. Mater.* **40** 349
[85] Dashevsky Z, Shufer E, Kasiyan V, Flitsiyan E and Chernyak L 2010 *Physica B* **405** 2380
[86] Urban J J, Talapin D V, Shevchenko E V, Kagan C R and Murray C B 2007 *Nat. Mater.* **6** 115
[87] Sootsman J R, Chung D Y and Kanatzidis M G 2009 *Angew. Chem. Int. Ed.* **48** 8616
[88] Hsu K F, Loo S, Guo F, Chen W, Dyck J S, Uher C, Hogan T, Polychroniadis E K and Kanatzidis M G 2004 *Science* **303** 818
[89] Hmood A, Kadhim A, Mahdi M A and Abu Hassan H 2016 *Int. J. Hydrogen Energy* **41** 5048
[90] Hogan T P, Downey A, Short J, Angelo J D and Wu C I 2007 *J. Electron. Mater.* **36** 704
[91] Ahn K, Kong H, Uher C and Kanatzidis M G 2016 *J. Solid State Chem.* **242** 34
[92] Falkenbach O, Schmitz A, Hartung D, Dankwort T, Koch G, Kienle L, Klar P J, Mueller E and Schlecht S 2016 *J. Appl. Phys.* **119** 214310
[93] Malhotra A and Maldovan M 2016 *J. Appl. Phys.* **120** 204305
[94] Yang L and Minnich A J 2017 *Sci. Rep.* **7** 44254
[95] Iskandar A, Aboukhalil A, Kazan M, Kassem W and Volz S 2015 *J. Appl. Phys.* **117** 125102
[96] Mascali G 2017 *J. Comput. Electron.* **16** 180
[97] Lu J, Guo R and Huang B 2016 *Appl. Phys. Lett.* **108** 141903
[98] Lindorf M, Rohrmann H, Span G, Raoux S and Jordansweet J 2016 *J. Appl. Phys.* **120** 205304
[99] Nozariasbmarz A, Rad A T, Zamanipour Z, Krasinski J S and Tayebi L 2013 *Scripta Mater.* **69** 549
[100] Rowe D J and Kortshagen U R 2014 *APL Mater.* **2** 22104
[101] Perez Taborda J A, Romero J J, Abad B, Ozrojo M M and Mello A 2016 *Nanotechnology* **27** 175401
[102] Zhu T, Fu C, Xie H, Liu Y and Zhao X 2015 *Adv. Energy Mater.* **5** 1500588
[103] Fu C, Zhu T, Liu Y, Xie H and Zhao X 2015 *Energy Environ. Sci.* **8** 216
[104] Fu C, Bai S, Liu Y, Tang Y and Chen L 2015 *Nat. Commun.* **6** 8144
[105] Wang S H, Cheng H M, Wu R J and Chao W H 2010 *Thin Solid Films* **518** 5901
[106] Shan R, Ouardi S, Fecher G H, Gao L, Kellock A, Gloskovskii A, Violbarbosa C E, Ikenaga E, Felser C and Parkin S S P 2012 *Appl. Phys. Lett.* **101** 212102
[107] Kozina X, Jaeger T, Ouardi S, Gloskowskij A, Stryganyuk G, Jakob G, Sugiyama T, Ikenaga E, Fecher G H and Felser C 2011 *Appl. Phys. Lett.* **99** 221908
[108] Jaeger T, Mix C, Schwall M, Kozina X, Barth J, Balke B, Finsterbusch M, Idzerda Y U, Felser C and Jakob G 2011 *Thin Solid Films* **520** 1010
[109] Zhou Y, Tan Q, Zhu J, Li S, Liu C, Lei Y and Li L 2015 *J. Electron. Mater.* **44** 1957
[110] Matsubara I, Funahashi R, Shikano M, Sasaki K and Enomoto H 2002 *Appl. Phys. Lett.* **80** 4729
[111] Diao Z, Lee H N, Chisholm M F and Jin R 2017 *Physica B* **511** 42
[112] Yan G, Bai Z, Wang S, Sun L and Wang J 2014 *Appl. Opt.* **53** 4211
[113] Zou D, Liu Y, Xie S, Lin J and Li J 2013 *Chem. Phys. Lett.* **586** 159
[114] Ohta S, Ohta H and Koumoto K 2006 *J. Ceram. Soc. Jpn.* **114** 102
[115] Ohta H, Kim S, Mune Y, Mizoguchi T and Nomura K 2007 *Nat. Mater.* **6** 129
[116] Liu S, Peng S, Ma J, Li G and Qin X 2017 *Superlattice. Microst.* **104** 282
[117] Lee S H, Lee J H, Choi S J and Park J S 2017 *Ceram. Int.* **43** 7784
[118] Nguyen N T, Nguyen T H, Liu Y R, Aminzare M and Pham A T 2016 *ACS Appl. Mater. Interfaces* **8** 33916
[119] Han L, Christensen D V, Bhowmik A, Simonsen S B, Hung L T, Abdellahi E, Chen Y Z, Nong N V, Linderoth S and Pryds N 2016 *J. Mater. Chem. A* **4** 12221
[120] Lee J, Park T, Lee S, Park N, Lee W, Lim J, Lee S and Park J 2016 *Ceram. Int.* **42** 14411
[121] Hoong L J, Keat Y C, Chik A and Leng T P 2016 *Ceram. Int.* **42** 12064
[122] He M, Qiu F and Lin Z 2013 *Energy Environ. Sci.* **6** 1352
[123] Kroon R, Mengistie D A, Kiefer D, Hynynen J, Ryan J D, Yu L and Muller C 2016 *Chem. Soc. Rev.* **45** 6147
[124] Shi H, Liu C, Jiang Q and Xu J 2015 *Adv. Electron. Mater.* **1** 1500017
[125] Culebras M, Gómez C and Cantarero A 2014 *Materials* **7** 6701
[126] Yang J, Yip H and Jen A K Y 2013 *Adv. Energy Mater.* **3** 549
[127] Wang L, Yao Q, Xiao J, Zeng K, Shi W, Qu S and Chen L 2016 *Chem. - Asian J.* **11** 1955
[128] Li J, Tang X, Li H, Yan Y and Zhang Q 2010 *Synth. Met.* **160** 1153
[129] Sun Y, Wei Z, Xu W and Zhu D 2010 *Synth. Met.* **160** 2371
[130] Yang W, Xu H, Li Y and Wang W 2017 *J. Electron. Mater.* **46** 4815
[131] Wang Y, Zhang S M and Deng Y 2016 *J. Mater. Chem. A* **4** 3554
[132] Wu J, Sun Y, Pei W B, Huang L and Xu W 2014 *Synth. Met.* **196** 173
[133] Culebras M, Uriol B, Gomez C M and Cantarero A 2015 *Phys. Chem. Chem. Phys.* **17** 15140
[134] Li C, Ma H and Tian Z 2017 *Appl. Therm. Eng.* **111** 1441
[135] Liang L, Gao C, Chen G and Guo C 2016 *J. Mater. Chem. C* **4** 526
[136] Du Y, Shen S Z, Cai K and Casey P S 2012 *Prog. Polym. Sci.* **37** 820
[137] Bubnova O, Khan Z U, Malti A, Braun S, Fahlman M, Berggren M and Crispin X 2011 *Nat. Mater.* **10** 429
[138] Khan Z U, Bubnova O, Jafari M J, Brooke R, Liu X, Gabrielsson R, Ederth T, Evans D R, Andreasen J W, Fahlman M and Crispin X 2015 *J. Mater. Chem. C* **3** 10616
[139] Wu F, Li P, Sun K, Zhou Y and Chen W 2017 *Adv. Electron. Mater.* **3** 1700047
[140] Yi C, Wilhite A, Zhang L, Hu R, Chuang S S C, Zheng J and Gong X 2015 *ACS Appl. Mater. Inter.* **7** 8984
[141] Kim N, Kee S, Lee S H, Lee B H, Kahng Y H, Jo Y, Kim B and Lee K 2014 *Adv. Mater.* **26** 2268
[142] Fan Z, Li P, Du D and Ouyang J 2017 *Adv. Energy Mater.* **7** 1602116
[143] Zhang S, Xia Y and Ouyang J 2017 *Org. Electron.* **45** 139
[144] Beretta D, Barker A J, Maqueira-Albo I, Calloni A, Bussetti G, Dell Erba G, Luzio A, Duó L, Petrozza A, Lanzani G and Caironi M 2017 *ACS Appl. Mater. Inter.* **9** 18151
[145] Cho C, Wallace K L, Tzeng P, Hsu J, Yu C and Grunlan J C 2016 *Adv. Energy Mater.* **6** 1502168
[146] Jiang F, Wang L, Li C, Wang X and Hu Y 2017 *J. Polym. Res.* **24** 68
[147] Zhang T, Li K, Li C, Ma S, Hng H H and Wei L 2017 *Adv. Electron. Mater.* **3** 1600554
[148] Jiang F, Xiong J, Zhou W, Liu C and Wang L 2016 *J. Mater. Chem. A* **4** 5265
[149] Zhou Y and Zhao L 2017 *Adv. Mater.* **29** 1702676
[150] Nakagawa J, Kage Y, Hori T, Shiomi J and Nomura M 2015 *Appl. Phys. Lett.* **107** 23104
[151] Zhou S, Qi M, Ai L, Xu A, Wang L, Ding P and Jin Z 2015 *Chin. Phys. Lett.* **32** 97101
[152] Shariati A, Rabani H and Mardaani M 2017 *Chin. Phys. B* **26** 36302
[153] Lee M, Ahn J, Sung J H, Heo H, Jeon S G, Lee W, Song J Y, Hong K, Choi B, Lee S and Jo M 2016 *Nat. Commun.* **7** 12011
[154] Cao L, Deng Y, Gao H, Wang Y, Chen X and Zhu Z 2015 *Phys. Chem. Chem. Phys.* **17** 6809
[155] Deng Y, Zhang Z, Wang Y and Xu Y 2012 *J. Nanopart. Res.* **14** 775